TERRAMECHANICS IMPACT OF THE WHEEL NORMAL REACTION ON MOBILITY AND STEERABILITY MARGINS

Jesse Paldan[1], Vladimir Vantsevich, PhD[1], David Gorsich, PhD[2], Jill Goryca[2], Amandeep Singh, PhD[2], Lee Moradi, PhD[1]

[1]The University of Alabama at Birmingham
[2]U.S. Army DEVCOM Ground Vehicle Systems Center

ABSTRACT

The normal reaction force in the tire-soil patch is a continuously changing wheel parameter. When a vehicle moves over uneven ground, motion in the vehicle's sprung and unsprung masses produce dynamic shifts in the magnitude of the load transmitted to the ground. With the damping force controlled for better ride quality, tight constraining of the sprung mass motion may lead to significant dynamic changes of the normal load. At excessive loads, the wheel can dig into the soil. Considerably reduced loads can negatively impact vehicle steerability and diminish traction performance. The purpose of this paper is to develop a method that allows for establishing boundaries of the dynamic normal reaction in the tire-soil patch on uneven terrain. The boundary constraints are considered for both maximum and minimum values to establish conditions for mobility and steerability. Using differential equations describing the motion two masses of a single-wheel module representing a vehicle corner, an inverse dynamics-based method is developed to recover a time history of the dynamic normal reaction of the wheel for assigned kinematics characteristics of the sprung mass and wheel longitudinal dynamics, and given stochastic characteristics of the terrain profile.

1. INTRODUCTION

The wheel normal dynamics has been established as having significant importance in wheeled vehicle dynamics. First, the wheel normal load has always been one of the essential parameters needed for selecting tires for vehicles. The tire loading characteristic—i.e., the functional relationship between the normal load and tire deflection—is essential for assessing the tire rolling resistance that is one of the crucial characteristics impacting tire power losses and, thus, vehicle fuel and energy consumption [1-3]. Nonlinearity of the loading characteristic makes the tire normal elasticity/stiffness variable which influences vehicle ride performance [4]. In terramechanics studies [5],

the normal load is modelled as the resultant of the stress distribution in the tire contact with deformable terrain and, thus, has a significant impact on the wheel sinkage, i.e., on vehicle terrain mobility.

The introduction of the vehicle corner as a two-mass system with sprung and unsprung masses played a pivotal role in vehicle dynamics development. Indeed, vibrational movements of the masses can result in the dynamic normal reaction in the tire patch that varies much, sometimes making it 3 to 4 fold bigger than the wheel load and in some cases going to zero when the wheel is lifting up [6]. This is especially true for off-road vehicles moving at higher speeds on unprepared terrain.

Dynamic variations of the normal reaction can impact longitudinal, lateral and rollover dynamics of a vehicle. Under substantial reduction of the normal reaction, tire grip properties can drastically drop and tire slippage can increase significantly and, thus, impact vehicle mobility [2, 7]. The variations in the normal reaction can reduce the tire ability to withstand external lateral forces (e.g., a centrifugal force in turn), which makes it difficult to steer the wheels properly and can lead to lateral skid of vehicle, especially on low friction surfaces [3]. Thus, suspension characteristics as well as the tire-soil loading characteristics become crucial not only for the ride design, but also for vehicle traction, mobility, stability of motion, and other vehicle operational properties. The gunfire accuracy of armored light vehicles drops significantly due to the rollover vibrations of the sprung mass, i.e., the vibrations about the longitudinal axis. For a vehicle rollover angle of 4 degrees and a gun elevation of 45 degrees, the deviation from the target is 9 m in the lateral direction and 0.45 m in the vertical direction when the distance to the target is 100 m [8].

There is a pretty common opinion that ride quality is less of a concern in autonomous vehicle design due to the absence of operators and passengers. However, as pointed out above, less advanced suspensions and tire-soil characteristics can significantly reduce autonomous vehicle performance in severe terrain conditions. Furthermore, there is one more technical issue that can be caused by significant changes in the wheel normal reaction. A wheel can be immobilized if the pressure in the tire-terrain contact exceeds the bearing capacity of the soil. Such a critical situation can be triggered by an increase of the wheel normal reaction, which in turn can occur due to high-speed motion on uneven terrain and active stabilization of the sprung mass. In this regards, in recent research, normal reaction observers were designed for real-time operation [9, 10]. The observation of the normal reaction allows for appropriate controlling of vehicle speed and suspension to avoid extreme increase of the pressure in the tire-soil contact.

At the same time, for the successful operation of the observers, actual observed values of the normal reaction need to be compared with some reference values that correspond to the bearing capacity of soil. For such purpose, this paper develops an analytical method to determine the reference values of the wheel normal reaction through simulations of a single-wheel module in various stochastic terrain conditions.

When utilizing a semi-active or active suspension to reduce or zero the sprung mass travel, two approaches are used 1) controlling the damping coefficient and 2) controlling the force in suspension. However, when the suspension forces are controlled to avoid motion of the sprung mass, the normal reaction drastically goes up. At high values of the normal reaction, the wheel sinkage increases and the pressure the tire exerts on the soil can reach its bearing capacity. The normal reaction also increases rolling resistance of the wheel, leading to a mobility problem. If the normal reaction is drastically reduced, a stability problem is raised since the wheel cannot develop lateral force well and thus the steerability becomes a problem. Additionally, the maximum traction forces are reduced when the normal reaction is low.

The goals of the paper are first to develop a method to model and simulate the normal reaction

Terramechanics Impact of the Wheel Normal Reaction on Mobility and Steerability Margins…, Paldan, et al.

Page 2 of 10

when limiting travel of the sprung mass. A virtual sensor that measures the suspension travel is used to determine the normal reaction in real time. Extreme values of the normal reaction are researched to establish boundaries for mobility and bearing capacity.

1. SINGLE WHEEL MODULE MODEL

The single wheel module used for this study is represented as a two-mass system linked by springs and dampers as shown in figure 1.
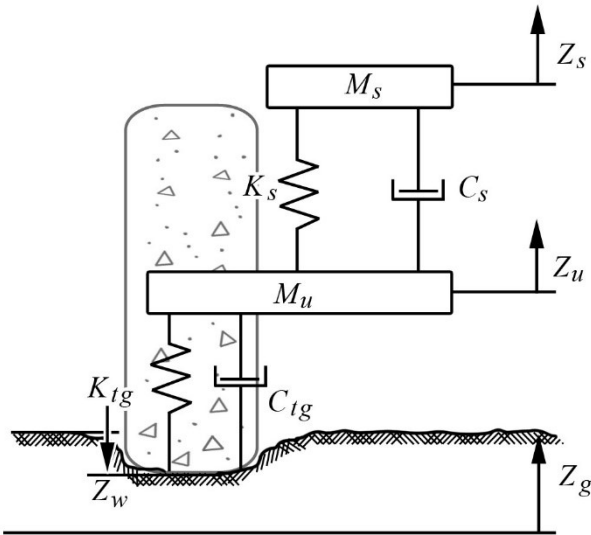

Figure 1: Two-mass model of single wheel module

1.1. Two Mass Oscillation Model

Masses m_s and m_u are the sprung and unsprung portions of the total vehicle corner mass. The suspension has a stiffness coefficient K_s and damping coefficient C_s. The tire has stiffness coefficient K_t and damping coefficient C_t. A ground stiffness and damping value are introduced to include the effect of the non-rigid surface on the oscillations. The tire stiffness is replaced with a combined stiffness of the tire and ground, K_{tg}. The stiffness of the soil can be much lower than the tire stiffness, especially in the first passage of the wheel before compaction of the soil by repeated passes [11].

$$K_{tg} = \frac{K_t K_g}{K_t + K_g} \tag{1}$$

The combined values are derived using the equation of two springs joined in series. The combined damping value is.

$$C_{tg} = \frac{C_t C_g}{C_t + C_g} \tag{2}$$

The equations for the oscillations of the two masses are derived using Lagrange's equations of the second kind. z_s and z_u are the vertical travel of the sprung and unsprung masses from their equilibrium positions when the wheel is stationary at zero ground height. The ground height z_g is the height of the surface profile. The equation describing the oscillation of the sprung mass is

$$m_s \ddot{z}_s - K_s(z_u - z_s) - C_s(\dot{z}_u - \dot{z}_s) = 0 \tag{3}$$

and the equation of the oscillation of the unsprung mass is

$$m_u \ddot{z}_u + K_s(z_u - z_s) - K_{tg}(z_g - z_u) + C_s(\dot{z}_u - \dot{z}_s) - C_{tg}(\dot{z}_g - \dot{z}_u) = 0 \tag{4}$$

The dynamic normal reaction is affected by the relative travel and velocity between the ground and the unsprung mass [3]

$$R_z = R_{z\_s} + K_{tg}(z_u - z_g) + C_{tg}(\dot{z}_u - \dot{z}_g) \tag{5}$$

where R_{z_s} is the static normal reaction that is equal to the weight of the wheel module.

1.2. Pressure Sinkage Model

Sinkage is the distance a wheel digs into the soil. The sinkage is linked to the pressure in the contact patch and normal reaction. Using Bekker's

Terramechanics Impact of the Wheel Normal Reaction on Mobility and Steerability Margins…, Paldan, et al.

Page 3 of 10

pressure-sinkage relationship, the sinkage is related to the pressure by [12]

$$z_w = \left(\frac{p_{gr}}{\frac{k_c}{b}+k_\phi}\right)^{\frac{1}{n}} \tag{6}$$

where p_{gr} is the average ground pressure, b is the smaller dimension of the contact patch (usually the tire width), and z_w is the wheel sinkage shown in figure 1. k_φ, k_c, and n are pressure-sinkage parameters obtainable by plate sinkage testing: k_c is a cohesive modulus of deformation, k_ϕ is a frictional modulus of deformation, and n is the pressure-sinkage exponent.

To solve for the sinkage of a flexible wheel with sinkage z_w and tire deflection δ_t as shown in figure 2 requires solving a group of equations [5].
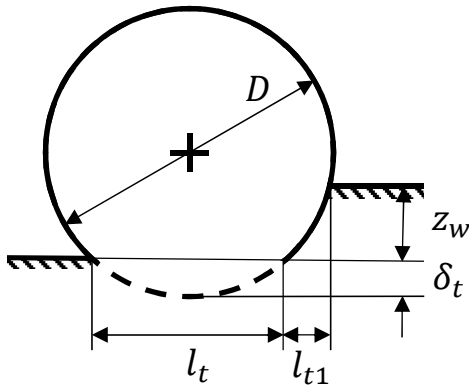

Figure 2: Sinkage and deflection of pneumatic tire [5]

The equilibrium for forces acting on the tire is

$$R_z = p_{gr}l_t b + W_{cu} \tag{7}$$

where W_{cu} is the component of the vertical reaction along the curved portion l_{t1} in figure 2. The reaction W_{cu} is calculated with

$$W_{cu} = l_t\left(\frac{k_c}{b}+k_\phi\right)\sqrt{D}(z_w+\delta_t)^{n-1} \times$$

$$\frac{\left[(3-n)(z_w+\delta_t)^{3/2}-(3-n)\delta_t^{\frac{3}{2}}-3z_w\sqrt{\delta_t}\right]}{3} \tag{8}$$

The contact length l_t is a function of the tire deflection δ_t.

$$l_t = 2\sqrt{D\delta_t - \delta_t^2} \tag{9}$$

The wheel sinkage is determined from equation (6). By solving equations (6-9) together with an iterative numeric method, a value of the sinkage is determined which satisfies the equilibrium of forces in equation (7).

1.3. Bearing Capacity

The bearing capacity of a tire whose contact length is greater than its width can be calculated using [13, 14]

$$W_s = A\left(cN_c + qN_q + 0.5\gamma bN_\gamma\right) \tag{10}$$

where A is the contact area, c is the coefficient of soil cohesion, and q is the surcharge load [13, 14]. The terms N_c, N_q, and N_γ are bearing capacity constants from Terzaghi's bearing capacity theory [14]. Terzaghi's bearing capacity theory was applied to vehicle terramechanics by Bekker [13]. The bearing capacity terms are dimensionless coefficients dependent on the soil's angle of internal friction ϕ alone; figure 3 shows the dependency of the N-factors on ϕ [13].
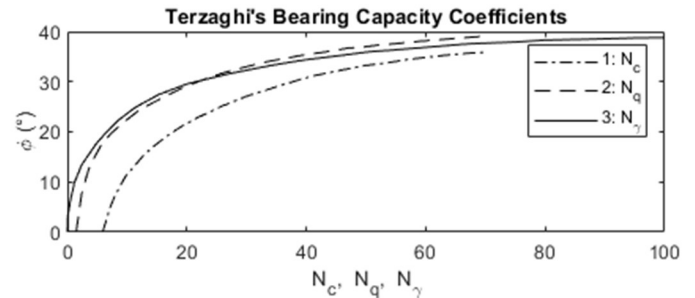

Figure 3: Terzaghi's bearing capacity coefficients [13]

Terramechanics Impact of the Wheel Normal Reaction on Mobility and Steerability Margins…, Paldan, et al.

Page 4 of 10

Equation (10) determines the safe load which does not cause soil failure by plastic flow [13]. The surcharge load q comes from accumulated soil when the wheel has sinkage:

$$q = \gamma z \qquad (11)$$

γ is the unit weight of soil. The surcharge arises from bulldozed soil displaced in the lateral direction on each side of the wheel [15, 16].

1.4. Circumferential force and Steerability

Minimum values of the normal reaction are utilized as the boundaries that limit the maximum circumferential wheel force and, thus, lead to excessive tire slippage and mobility loss if the resistance to motion requires more traction than the wheel can provide due to reduced friction with the ground. The friction coefficient of the wheel is [3]

$$\mu_x = \frac{F_x}{R_z} \qquad (12)$$

where F_x is the wheel's circumferential force. For the wheel to move at an assigned velocity, the circumferential force must be able to match the corresponding motion resistance $R_{m\Sigma}$, which includes rolling resistance, inertia force in translational motion, gravity component on a hill, etc. A slippage curve is shown in figure 4.
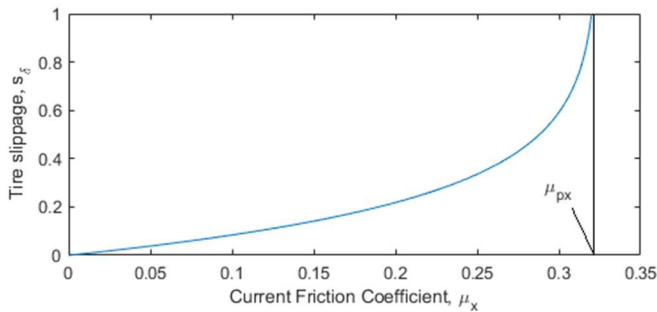

Figure 4: Current and peak friction coefficients μ_x and μ_{px}

As the current friction coefficient μ_x increases, the tire slippage increases exponentially. The maximum value of μ_x is limited by the peak friction

coefficient μ_{px}, which μ_x approaches asymptotically. Based on equation (12) and figure 4, the minimum boundary of the normal reaction R_z^{min} is assigned which would allow F_x to reach $R_{m\Sigma}$ for a given value of μ_{px}:

$$\mu_{px} R_z^{min} > R_{m\Sigma} \qquad (13)$$

The value of μ_{px} is a property of the tire and terrain which varies stochastically. When condition (13) is not satisfied, the wheel is immobilized. When $R_z^{min} < 0.2 R_{z\_s}$, the wheel is hardly steerable.

2. INVERSE DYNAMICS FORMULATION

An inverse dynamics problem was formulated and solved to recover a stochastic force that acts on the sprung and unsprung masses. The relative movement of the sprung and unsprung masses are measured by a virtual sensor.

$$L = (z_s - z_u). \qquad (14)$$

To allow a method that is indifferent to the tire-terrain dynamic interaction, since the stiffness and damping coefficients of the tire-terrain patch are usually difficult to obtain in online mode, the equation of the normal reaction is transformed into a function of L.

$$R_z = R_{z\_s} + m_u \ddot{L} + \left(\frac{m_u}{m_s} + 1\right)\left(C_s \dot{L} + K_s L\right) \qquad (15)$$

In reference [9], a sliding mode observer to estimate the dynamic normal reaction using the relative displacement sensor measurement L was developed and shown to be indifferent to variation of the stiffness and damping coefficients of tire-surface coupling and therefore applicable to any terrain.

Two methods of damping were considered for stabilizing the motion of the sprung mass: one by varying the suspension damping coefficient (semi-

Terramechanics Impact of the Wheel Normal Reaction on Mobility and Steerability Margins…, Paldan, et al.

Page 5 of 10

active damping), and a second by applying a damping force (active damping).

For the semi-active case, if the sprung mass equation is solved for the damper characteristic C_s, the following result is obtained

$$C_s = \frac{1}{\dot{L}}(\ddot{z}_s m_s - K_s L) \qquad (16)$$

By setting $\ddot{z}_s$ to zero, the variable damping constant to fully stabilize the mass is obtained. Fully stabilizing the mass has the condition that $\dot{L} \neq 0$ and $C_s \geq 0$ because the damping force is proportional to velocity and a negative damping coefficient is not possible.

In the active damping case, the suspension damping $C_s(\dot{z}_u - \dot{z}_s)$ is replaced with suspension damping force F_{sd}. The equations of the masses and normal reaction become

$$m_s \ddot{z}_s - K_s(z_u - z_s) - F_{sd} = 0 \qquad (17)$$
$$m_u \ddot{z}_u + K_s(z_u - z_s) + F_{sd} - K_{tg}(z_g - z_u) - C_{tg}(\dot{z}_g - \dot{z}_u) = 0 \qquad (18)$$
$$R_z = R_{z\_s} + m_u \ddot{L} + \left(\frac{m_u}{m_s} + 1\right)(K_s L - F_{sd}) \quad (19)$$

The value of F_{sd} to keep the sprung mass acceleration equal to zero can be obtained from equation (17) when setting $\ddot{z}_s = 0$:

$$F_{sd} = -K_s(z_u - z_s) = K_s L \qquad (20)$$

Two simulation cases are examined in this study: a wheel with passive damping and the same wheel with the suspension damping force from equation (20) used to avoid motion of the sprung mass. The effect of the active damping on the wheel normal reaction, and its implications for wheel mobility, is then considered in section 3.

3. STOCHASTIC TERRAIN SIMULATION

A computer simulation of the inverse dynamics problem was performed on a model of a single wheel module with characteristics given in table 1.

Table 1: Single wheel module characteristics

Sprung mass	m_s	1221.7 kg
Unsprung mass	m_u	180.00 kg
Suspension stiffness	K_s	200 kN/m
Suspension damping (passive suspension)	C_s	50 kNs/m
Tire stiffness	K_t	397.45 kN/m
Tire damping	C_t	3.9745 kNs/m
Ground stiffness	K_g	34.667 kN/m
Ground damping	C_g	0.3467 kNs/m
Tire/ground stiffness	K_{tg}	31.886 kN/m
Tire/ground damping	C_{tg}	0.31886 kNs/m

The wheel moves at a constant linear velocity of 40 kph (11.1 m/s). The simulation was performed on stochastic terrain with a varying height profile and peak coefficient of friction. Terramechanics does not offer data on the stochastic variance of the peak friction coefficient, so a method was used to generate simulation values for demonstration purposes only. Due to the lack of this data, as a first approximation, the peak friction coefficient was modeled as a random process correlated with the terrain micro-profile [17]. It is assumed that terrain hollows accumulate more moisture and thus the peak friction coefficient in dips is lower compared with its values at humps [17]. The height profile and stochastic peak friction coefficient are shown in figure 5 for a 10 m section of generated soil terrain.
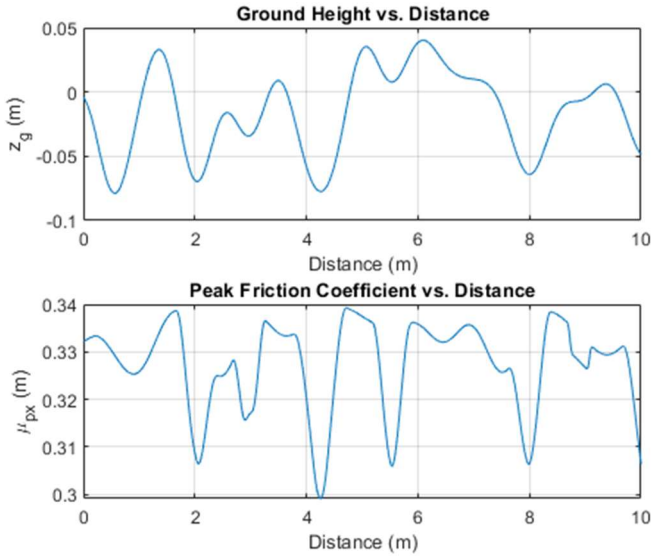
Terramechanics Impact of the Wheel Normal Reaction on Mobility and Steerability Margins…, Paldan, et al.

Page 6 of 10

Figure 5: Height profile and stochastic peak friction coefficient for soil terrain

Soil strength and pressure-sinkage parameters used for the sinkage and bearing capacity equations are given in table 2 [18]. These parameters were obtained from plate sinkage and Cohron sheargraph tests on Norfolk sandy loam soil.

Table 2: Norfolk Sandy Loam soil parameters [18]

Cohesion	c	15.06 kPa
Internal friction angle	φ	8.37°
Cohesive modulus of deformation	k_c	5.27 kN/m^{n+1}
Frictional modulus of deformation	k_φ	1015.04 kN/m^{n+2}
Pressure-sinkage exponent	n	0.8
Unit weight of soil	γ	11.8701 kN

The damping or force needed to make the sprung mass acceleration equal to zero are shown in figures 6 and 7. for a 10 second simulation.
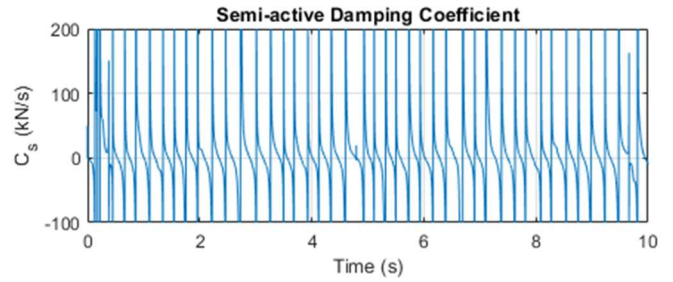

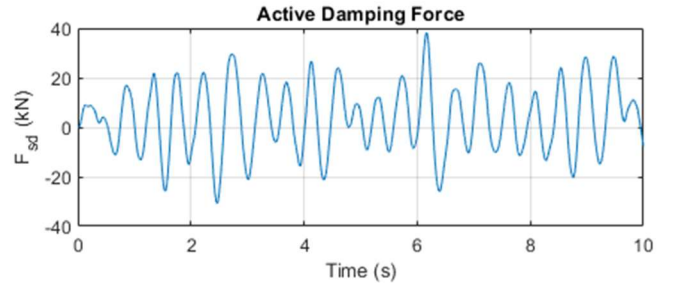**Figure 6**: Semi-active damping coefficient to fully stabilize sprung mass

Figure 7: Active damping coefficient to fully stabilize sprung mass

The variable damping plot in figure 7 shows occurrence of unrealistic high and negative damping values, making it insufficient to fully stabilize the sprung mass at all times. The force produced from the damping constant is proportional to velocity, making it unable to produce force when the velocity drops to zero. The histograms in figure 8 show how often the values occur.
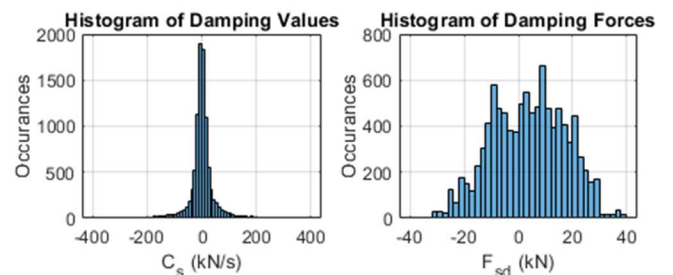

Figure 8: Histogram of damping coefficients (semi-active damping, left) and damping forces (active damping, right)

For the semi-active damping, for the majority of the time the damping coefficient does not need to exceed 50 Ns/m. In control systems of semi-active suspensions, when the required damping

Terramechanics Impact of the Wheel Normal Reaction on Mobility and Steerability Margins…, Paldan, et al.

Page 7 of 10

coefficient would be negative, the damping force is instead controlled to its minimum level [19].

Figures 9-10 show the travel and acceleration of the sprung and unsprung mass. Numbered lines pointing to curves on the plot identify corresponding entries in the plot legend.
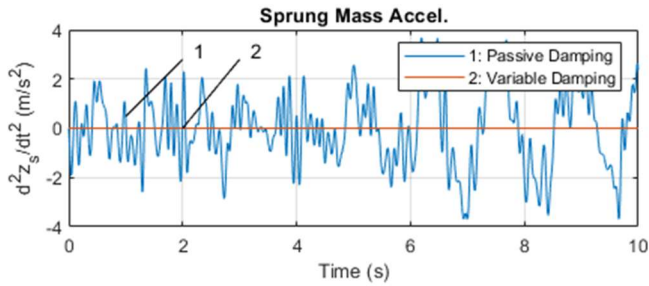

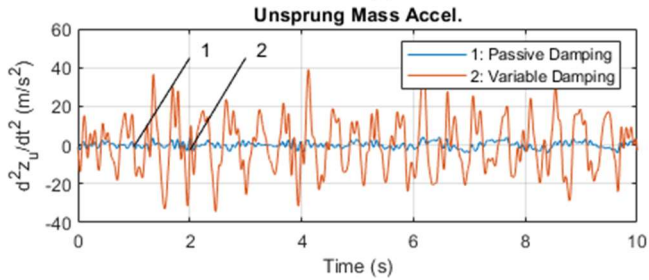**Figure 9:** Sprung mass acceleration

Figure 10: Unsprung mass acceleration

When the sprung mass is fully stabilized at zero acceleration, it greatly increases the acceleration of the unsprung mass. The motion of the unsprung mass contributes to the dynamic changes in the normal reaction (see equation 5).

The dynamic normal reaction is shown in figure 11 for the passive damping case and in figure 12 for the variable damping cases.
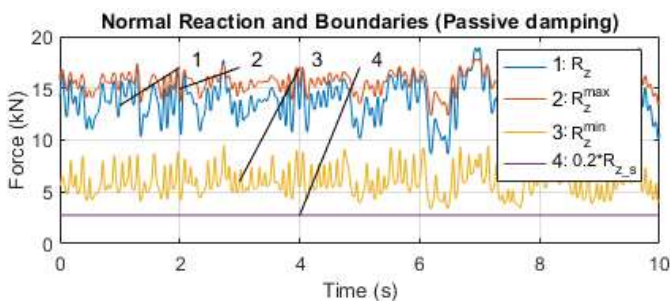

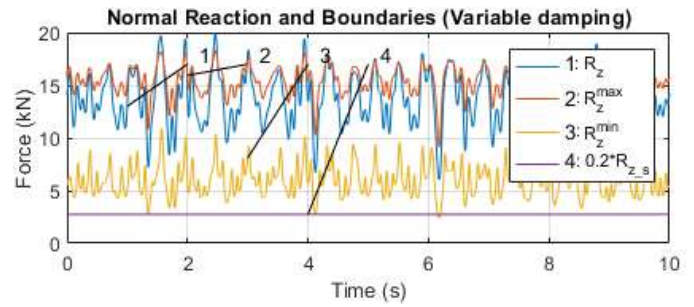**Figure 11**: Dynamic normal reaction (passive damping)

Figure 12: Dynamic normal reaction (variable damping)

The maximum boundary of the normal reaction is the bearing capacity from equation 10. The minimum boundary is the obtained from condition 13. As seen in figure 12, fully stabilizing the sprung mass also results in greater dynamic changes of R_z. This causes more incidences of R_z exceeding the bearing capacity as well as drops which approach the minimum value R_z^{min} for mobility. In neither case did the normal reaction approach the boundary of $0.2R_{z\_s}$ for steerability. At most moments of time, the minimum boundary for mobility would also satisfy the minimum boundary for steerability, but R_z^{min} can drop below $0.2R_{z\_s}$ as seen at 4.1 s and 6.2 s of the variable damping case.

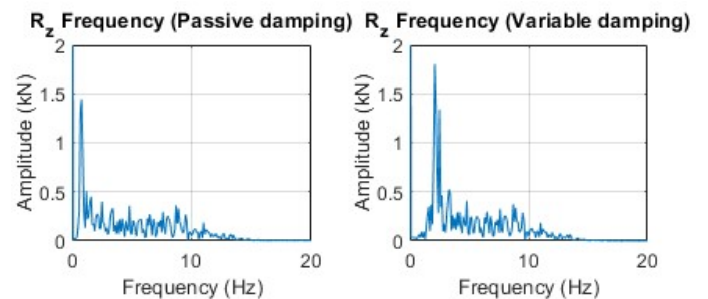Figure 13 is a frequency domain plot of the normal reaction.

Figure 13: Normal reaction (frequency domain)

The amplitude at 0 Hz indicates the mean value, which is close to the static normal reaction of 13.751 kN. A peak indicates frequencies at which most of the dynamic changes occur, which is at 0.80 Hz for the passive damping case with an amplitude of 1.44 kN. In the variable damping case,

Terramechanics Impact of the Wheel Normal Reaction on Mobility and Steerability Margins…, Paldan, et al.

Page 8 of 10

two peaks occur at higher frequencies: one at 2.10 Hz with an amplitude of 1.80 kN, and one at 2.50 Hz with an amplitude of 1.34 kN.

4. CONCLUSION

A method was developed to determine boundaries of the wheel normal reaction. The upper boundary is based on the bearing capacity which leads to soil damage when exceeded by the dynamic load in the tire-ground contact patch. The minimum boundaries are obtained from minimum values of the normal reaction required for traction and steerability. Using an inverse dynamics method, the values of the dynamic normal reaction are obtained when a semi-active or active damper is used to stop oscillation of the sprung mass. The normal reaction can be determined from the relative travel of the sprung and unsprung masses. Simulation results in stochastically-varying terrain demonstrate the calculation of the boundaries and the effect of zeroing the sprung mass acceleration on the normal reaction. When the sprung mass is held steady, the dynamic changes in the normal reaction are increased. When controlling the suspension damping forces, the goals of stabilizing the sprung mass, avoiding exceeding the soil bearing capacity, and maintaining sufficient normal reaction for mobility and steerability must be kept in balance. To facilitate this, reference values of the normal reaction will be used to build a database needed for an AI-decision making system integrated with a wheel control. As part of the construction of this database, the demonstrated method will be applied across additional terrains, vehicle sizes, and soil parameters.

5. REFERENCES

[1] T. D. Gillespie, *Fundamentals of Vehicle Dynamics*, SAE, 1992, 495 pages.

[2] V. V. Larin, *Theory of motion of all-wheel drive vehicles*, Publisher of Moscow State Technical University n.a. Bauman, Moscow, 2010, 391 pages (in Russian).

[3] A. F. Andreev, V. I. Kabanau, V. V. Vantsevich, *Driveline of Ground Vehicles: Theory and Design*, Taylor and Francis Group/CRC Press, 2010.

[4] J. Dixon, *Tires, Suspension, and Handling,* 2nd edition, SAE, 1996, 621 pages.

[5] J. Y. Wong, *Theory of Ground Vehicles*, Third Edition, John Wiley & Sons, 2001.

[6] V.F. Platonov, *All-Wheel Drive Vehicles*, Mashinostroenie Publisher, Moscow, 1989, 308 pages (in Russian).

[7] N. S. Vol'skaya, *Wheeled Vehicle Mobility Assessment on non-Even Terrain Surface*, Publisher of Moscow State Technical University n.a. Bauman, Moscow, 2007, 215 pages (in Russian).

[8] B. A. Mel'nik, "ON THE QUESTION OF THE INFLUENCE OF ROLLOVER VIBRATIONS OF THE SPRUNG MASS OF LIGHT ARMORED WHEELED VEHICLES ON THE ACCURACY OF GUNFIRE", *Mechanics and Machine Building*, N2, 2012, pp. 118 - 121 (in Russian).

[9] L. Zhao, V. V. Vantsevich, "A Robust Estimation of Dynamic Normal Reaction for Open-Link Locomotion Module with an E-drive", *Int. J. Vehicle System Dynamics*, 2019, doi: 10.1080/00423114.2019.1627468.

[10] V. V. Vantsevich, D. Gorsich, A. Lozynskyy, L. Demkiv, T. Borovets, "State Observers for Terrain Mobility Controls: A Technical Analysis", *IFToMM Congr*., Krakow, Poland, 2019.

[11] Smirnov G.A., *Theory of motion of wheeled vehicles*, 2nd edition, Moscow, Mashinostroenie publishing house, 1990, 352 pages (in Russian).

[12] J. Y. Wong, *Terramechanics and Off-Road Vehicle Engineering*, Butterworth-Heinemann, 2010.

[13] M. G. Bekker, *Theory of land Locomotion: The Mechanics of Vehicle Mobility*, Ann Arbor: University of Michigan Press, 1956.

Terramechanics Impact of the Wheel Normal Reaction on Mobility and Steerability Margins…, Paldan, et al.

Page 9 of 10

[14] S. Laughery, G. Gerhart, P. Muench, "Evaluating Vehicle Mobility Using Bekker's Equations", US Army TARDEC, 2000.

[15] C. Senatore, C. Sandu, "Off-Road Tire Modeling and the Multi-Pass Effect For Vehicle Dynamics Simulation", *J. Terramechanics*, Volume 48, Issue 4, 2011.

[16] C. Sandu, E. Pinto, S. Naranjo, P. Jayakumar , A. Andonian, D. Hubbell, B. Ross, "Off-Road Soft Soil Tire Model Development and Experimental Testing", *17th Int. Conf. Int. Society Terrain-Vehicle Systems*, 2011.

[17] J. P. Gray, V. V. Vantsevich, A. F. Opeiko, and G. R. Hudas, "A Method for Unmanned Ground Wheeled Vehicle Mobility Estimation in Stochastic Terrain Conditions," *Proc. 7th Americas Regional Conf. ISTVS,* 2013.

[18] M. A. Salama, T. R. Way, V. V. Vantsevich, "Parameterization of Norfolk Sandy Loam Properties for Stochastic Modeling of Light In-Wheel Motor UGV", *Proc. 8th Americas Regional Conf. Int. Society Terrain Vehicle Systems*, 2016.

[19] I. Naoki, "Semi-active Suspension", KYB TECHNICAL REVIEW No. 55, 2017.

Terramechanics Impact of the Wheel Normal Reaction on Mobility and Steerability Margins…, Paldan, et al.

Page 10 of 10